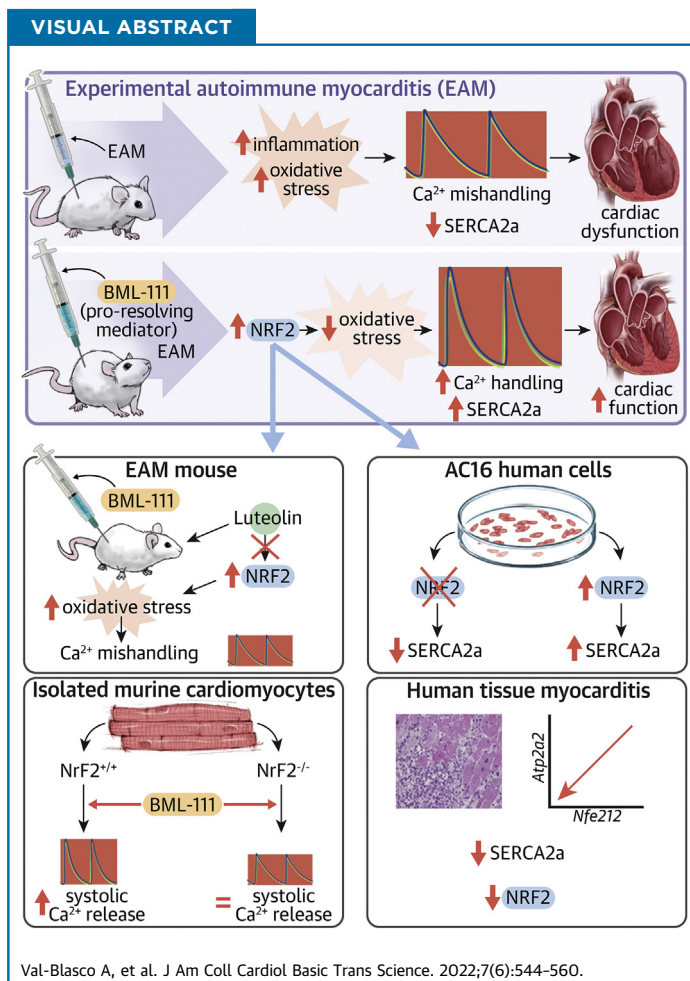**PRECLINICAL RESEARCH**

Specialized Proresolving Mediators Protect Against Experimental Autoimmune Myocarditis by Modulating Ca^{2+} Handling and NRF2 Activation

Almudena Val-Blasco, PhD,[a,b,*] Patricia Prieto, PhD,[c,d,*] Rafael Iñigo Jaén, BSc,[e,*] Marta Gil-Fernández, BSc,[a,e,*] Marta Pajares, PhD,[e,f,†] Nieves Domenech, PhD,[d,g,†] Verónica Terrón, BSc,[a] María Tamayo, PhD,[e] Inmaculada Jorge, PhD,[d,h] Jesús Vázquez, PhD,[d,h] Andrea Bueno-Sen, BSc,[a] María Teresa Vallejo-Cremades, PhD,[i] Jorge Pombo-Otero, MD,[g] Sergio Sanchez-García, BSc,[e] Gema Ruiz-Hurtado, PhD,[d,j] Ana María Gómez, PhD,[b] Carlos Zaragoza, PhD,[d,k] María Generosa Crespo-Leiro, MD, PhD,[d,g] Eduardo López-Collazo, PhD,[a,l] Antonio Cuadrado, PhD,[a,e,f,m] Carmen Delgado, PhD,[d,e] Lisardo Boscá, PhD,[d,e] María Fernández-Velasco, PhD[a,d]

VISUAL ABSTRACT

Val-Blasco A, et al. J Am Coll Cardiol Basic Trans Science. 2022;7(6):544–560.

HIGHLIGHTS

- Administration of BML-111, a stable LXA4 analog, protects against cardiac dysfunction by avoiding Ca^{2+} mishandling induced by autoimmune myocarditis in a mouse model.

- Beneficial effects of the SPMs on intracellular Ca^{2+} handling are mainly caused by a regulation of SERCA2A by NRF2.

- Cardiac tissue obtained from individuals diagnosed with myocarditis, compared with healthy myocardium tissues, displayed depressed mRNA levels of *ATP2A2* (SERCA2A) and *NF2L2* (NRF2).

SUMMARY

Specialized proresolving mediators and, in particular, 5(S), (6)R, 7-trihydroxyheptanoic acid methyl ester (BML-111) emerge as new therapeutic tools to prevent cardiac dysfunction and deleterious cardiac damage associated with myocarditis progression. The cardioprotective role of BML-111 is mainly caused by the prevention of increased oxidative stress and nuclear factor erythroid-derived 2-like 2 (NRF2) down-regulation induced by myocarditis. At the molecular level, BML-111 activates NRF2 signaling, which prevents sarcoplasmic reticulum–adenosine triphosphatase 2A down-regulation and Ca²⁺ mishandling, and attenuates the cardiac dysfunction and tissue damage induced by myocarditis. (J Am Coll Cardiol Basic Trans Science 2022;7:544–560) © 2022 The Authors. Published by Elsevier on behalf of the American College of Cardiology Foundation. This is an open access article under the CC BY-NC-ND license (http://creativecommons.org/licenses/by-nc-nd/4.0/).

**ABBREVIATIONS
AND ACRONYMS**

8OHdG = 8-hydroxy-2'-deoxyguanosine

BML-111 = 5(S), (6)R, 7-trihydroxyheptanoic acid methyl ester

Ctrl = control

Cys = cysteine

EAM = experimental autoimmune myocarditis

EC = excitation-contraction

Epi = 15-epi-lipoxin A4

Lut = luteolin

LXA4 = lipoxin A4

mRNA = messenger RNA

NRF2 = nuclear factor erythroid-derived 2-like 2

SCR = spontaneous diastolic Ca²⁺ release

SERCA2A = sarcoplasmic reticulum-adenosine triphosphatase 2A

SPM = specialized proresolving mediator

SR = sarcoplasmic reticulum

Veh = vehicle

Myocarditis is an inflammatory disease of the myocardium caused by infectious and noninfectious agents and is considered a precursor of dilated cardiomyopathy.[1] Myocarditis has recently been identified in severe forms of COVID-19 and can worsen the prognosis of patients infected with SARS-CoV-2.[2]

Myocarditis has a heterogeneous clinical course, ranging from asymptomatic forms to acute coronary syndromes, including new-onset heart failure, cardiac arrhythmias, or chronic heart failure.[3] Many of these features have been associated with mishandling of intracellular Ca²⁺,[4] which is a key factor in the regulation of excitation-contraction (EC)-coupling controlling muscle contraction in the heart. EC-coupling is initiated by an action potential in cardiomyocytes that stimulates a small influx of Ca²⁺ via sarcolemma L-type Ca²⁺ channels. Entry of Ca²⁺ into the cytosol triggers a large release of Ca²⁺ from the sarcoplasmic reticulum (SR) through ryanodine receptors (RyR2), resulting in increased intracellular Ca²⁺ concentrations that activate myofilaments, prompting cell contraction.[5] Relaxation is achieved by reuptake of Ca²⁺ into the SR by sarcoplasmic reticulum-adenosine triphosphatase 2A (SERCA2A), and across the plasma membrane by the Na⁺/Ca²⁺ exchanger. SERCA2A activation is highly regulated by the small protein phospholamban. Ca²⁺ mishandling is closely associated with cardiac dysfunction and arrhythmias, but little is known about EC-coupling in the physiopathology of myocarditis.[6]

The different etiologies of myocarditis together with challenges in diagnosis caused by heterogeneity in clinical presentation limit the options for treatment. In many cases, patients with acute myocarditis are treated for heart failure, but they can also be treated with immunosuppressants, antivirals (including interferon beta), nonsteroidal anti-inflammatory drugs, or colchicine depending on symptomatology.[1] Thus, efforts to develop more specific therapeutic modalities are required. Given that the pathologic phenotype of myocarditis is typically related to cardiac inflammation, specific mediators that promote the resolution

From the ᵃInnate Immune Response Group, La Paz University Hospital, Instituto de Investigación Biomédica del Hospital La Paz (IdiPAZ), Madrid, Spain; ᵇSignaling and Cardiovascular Pathophysiology, Unite Mixte de Recherche S 1180, Institut National de la Santé et de la Recherche Médicale, Université Paris-Saclay, Paris, France; ᶜPharmacology, Pharmacognosy, and Botany Department, Faculty of Pharmacy, Complutense University of Madrid, Madrid, Spain; ᵈCentro de Investigación Biomédica en Red de Enfermedades Cardiovasculares (CIBERCV), Madrid, Spain; ᵉInstituto de Investigaciones Biomédicas "Alberto Sols," Consejo Superior de Investigaciones Científicas, Autonomous University of Madrid (UAM), Madrid, Spain; ᶠCentro de Investigación Biomédica en Red Sobre Enfermedades Neurodegenerativas, Madrid, Spain; ᵍInstituto de Investigación Biomédica de A Coruña, Complexo Hospitalario Universitario de A Coruña, Sergas, Universidad da Coruña, A Coruña, Spain; ʰCentro Nacional de Investigaciones Cardiovasculares, Madrid, Spain; ⁱMolecular Image and Immunohistochemistry Unit, IdiPAZ, La Paz University Hospital, Madrid, Spain; ʲCardiorenal Translational Laboratory, Institute of Research i+12, CIBERCV, Hospital Universitario 12 de Octubre, Madrid, Spain; ᵏDepartamento de Cardiología, Unidad de Investigación Mixta Universidad Francisco de Vitoria, Madrid, Spain; ˡCentro de Investigación Biomédica en Res de Enfermedades Respiratorias, Madrid, Spain; and the ᵐDepartment of Biochemistry, Faculty of Medicine, UAM, Madrid, Spain. *Drs Val-Blasco, Prieto, Jaén, and Gil-Fernández contributed equally to this work and are joint first authors. †Drs Pajares and Domenech contributed equally to this work and are joint second authors. The authors attest they are in compliance with human studies committees and animal welfare regulations of the authors' institutions and Food and Drug Administration guidelines, including patient consent where appropriate. For more information, visit the Author Center.

Manuscript received July 20, 2021; revised manuscript received January 21, 2022, accepted January 23, 2022.

of inflammation, such as specialized proresolving mediators (SPMs), are relevant candidates for research.

SPMs were first elucidated by Serhan and Savill[7] as eicosanoids that dominate the resolution phase of inflammation and help to re-establish tissue homeostasis.[8] The fatty acid arachidonic acid is the precursor of some of the most studied SPMs, termed lipoxins, that exert their actions principally through engagement with the G protein-coupled receptor FPR2/ALXR. Lipoxins are SPMs enzymatically formed by transcellular biosynthesis via 3 different routes: 2 of which are endogenous pathways for lipoxin A4 (LXA4) and LXB4 biosynthesis, and a third pathway that, in the presence of aspirin, generates epi-derivatives of lipoxins known as 15-epi-lipoxin A_4/B_4. These "aspirin-triggered lipoxins" retain the main actions of native compounds but with significantly increased potency. Because of their short half-life and rapid inactivation in vivo, several synthetic derivatives of native lipoxins have been developed such as the LXA4 receptor agonist 5(S), (6)R, 7-trihydroxyheptanoic acid methyl ester (BML-111) (Supplemental Figure 1), which has improved stability and potency in vivo.[9]

SPMs can prevent the development of chronic inflammation and temper the formation of oxidative stress, and many of their beneficial effects have been attributed to the inhibition of the proinflammatory nuclear factor-kB pathway and to the activation of the antioxidant factor nuclear factor erythroid-derived 2-like 2 (NRF2).[8]

NRF2 is a transcription factor that can directly and indirectly activate the expression of anti-inflammatory genes and also induces the transcriptional repression of some proinflammatory genes.[10] NRF2 may counteract inflammation indirectly by modulating oxidative stress pathways, such as those governed by NQO1 and heme oxygenase 1, leading to an anti-inflammatory response. Although the cardioprotective role of NRF2 has been extensively studied,[11] whether it is involved in the beneficial SPM-mediated cardiac effects through the regulation of intracellular Ca²⁺ dynamics is unknown.

In the present study, we investigated whether administration of BML-111 in an experimental autoimmune myocarditis (EAM) model in mice prevents cardiac dysfunction and intracellular Ca²⁺ mishandling via NRF2 activation.

METHODS

ANIMALS. The present study was conducted following the guidelines of the Spanish Animal Care and Use Committee according to the European Union (2010/63/EU) and conformed to the Guide for the Care and Use of Laboratory Animals Published by the U.S. National Institute of Health (NIH Publication No 85-23, revised 1996). The study was approved by the Bioethics Committee of the Community of Madrid (PROEX 144/17).

HUMAN SAMPLES. Endomyocardial biopsies were obtained from patients who developed myocarditis (defined according to the American College of Cardiology and American Heart Association clinical guidelines). All samples were obtained from excess tissue initially extracted for clinical diagnosis. Biopsies were obtained from healthy donors' hearts from Biobanco A Coruña (Cod.0000796). The 8 patients with myocarditis (6 male and 2 female) had a median age of 31 years. The 5 healthy myocardium donors (4 male and 1 female) had a median age of 56 years. The study was conducted according to Spanish Law for Biomedical Research (Law 14/2007-3 of July) and was compliant with the Declaration of Helsinki. The study and the use of samples were approved by the Research Ethics Committee of Galicia (Ref 2017/541). Written informed consent was obtained from all patients.

STATISTICS. The values shown in graphs correspond to the mean ± SD. Differences between group mean values were estimated with the 2-tailed Student's *t*-test for unpaired observations, and more than 2 groups were compared using 1-way analysis of variance followed by Tukey's post hoc test for multiple comparisons, as indicated. In the proteomics analysis, outliers at the peptide and protein levels were detected at 1% false discovery rate and results of modified cysteine (Cys)-containing peptide abundance changes were tested for significance using the Kolmogorov-Smirnov test. A value of $P \leq 0.05$ was considered statistically significant. All analyses were performed using GraphPad Prism Software.

Expanded Methods are provided in the Supplemental Appendix.

RESULTS

STRUCTURAL AND FUNCTIONAL CARDIAC CHARACTERIZATION OF MICE WITH INDUCED EAM AND THE EFFECTS OF BML-111. Infiltrated immune cells are commonly found in the myocardium of patients with myocarditis. Hematoxylin-eosin staining demonstrated that mice treated with α-myosin heavy chain and vehicle (EAM+Veh) had more immune cell infiltration in the myocardium than vehicle-treated control mice (Ctrl+Veh) did (Figure 1B), as expected in EAM model. Cardiac expression of the

FIGURE 1 **BML-111 Administration Prevents Cardiac Dysfunction and Systolic Ca^{2+} Dysregulation in EAM-induced Mice**
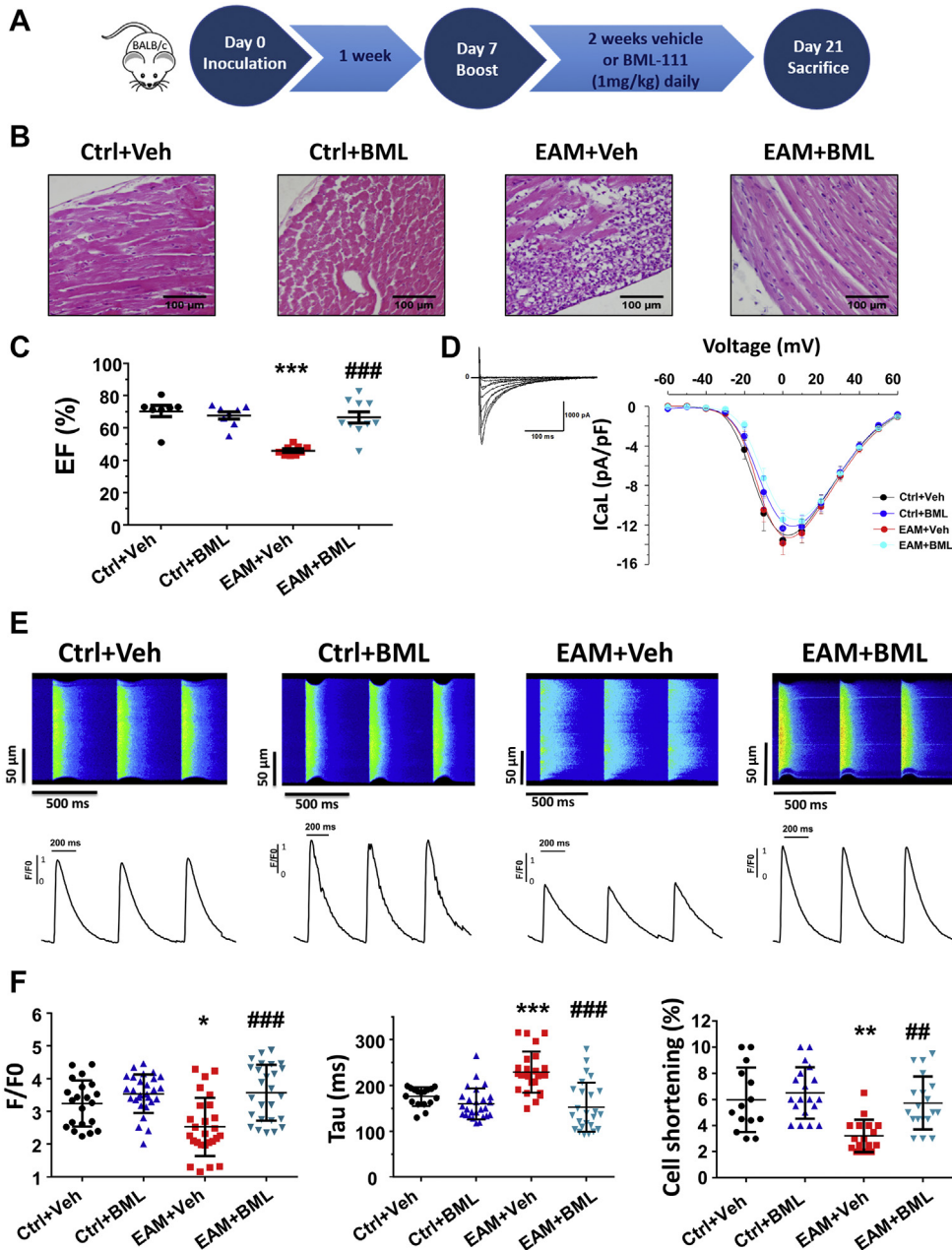
(A) Experimental design. **(B)** Representative hematoxylin and eosin–stained slides of hearts from control + vehicle, (Ctrl+Veh), control + 5(S), (6)R, 7-trihydroxyheptanoic acid methyl ester (BML-111) (Crtl+ BML), experimental autoimmune myocarditis (EAM) + vehicle (EAM+Veh), and EAM + BML-111 (EAM+BML)-treated mice. Original magnification ×20. **(C)** Individual and mean values of ejection fraction (EF) in Ctrl+Veh (N = 7), Ctrl+BML (N = 8), EAM+Veh (N = 9), and EAM+BML (N = 10) mice. **(D, left)** Representative traces of calcium influx through L-type channels (I$_{CaL}$) obtained from −60 to +60 mV acquired in a cardiomyocyte from a vehicle-treated mouse. **(Right)** Mean density values of I$_{CaL}$ recorded at all voltages tested in cardiomyocytes from Ctrl+Veh (N = 16, N = 4), Ctrl+BML (N = 18, N = 3), EAM+Veh (N = 12, N = 5), and EAM+BML (N = 18, N = 4) groups. **(E)** Representative line-scan confocal images and the corresponding profiles of Ca^{2+} transients from 1 cell in each experimental group. **(F)** Individual and mean values of peak fluorescence Ca^{2+} transients **(left)**, the decay time constant (Tau) **(center)**, and cell shortening **(right)** obtained in cardiomyocytes from Ctrl+Veh (N = 21, N = 5), Ctrl+BML (N = 28, N = 4), EAM+Veh (N = 26, N = 4), and EAM+BML (N = 26, N = 4) mice. Data show individual values and mean ± SD. *$P < 0.05$, **$P < 0.01$, and ***$P < 0.001$ versus Ctrl+Veh; and ##$P < 0.01$ and ###$P < 0.001$ versus EAM+Veh.

TABLE 1   Cardiac Expression of Proinflammatory Cytokines and Indicators of Cardiac Hypertrophy

	Il1b (FI)	*Tnfa* (FI)	HW/TL Ratio	Cell Surface (μm²)	*Nppa* (FI)	HR (beats/min)	N
Ctrl+Veh	0.79 ± 0.1	0.81 ± 0.3	7.2 ± 0.9	2,556 ± 283.9	0.82 ± 0.3	305.1 ± 49.3	6
Ctrl+BML	0.75 ± 0.2	1.09 ± 0.3	7.5 ± 0.8	2,412 ± 464.9	0.64 ± 0.2	300.5 ± 37.9	6
EAM+Veh	1.93 ± 0.7[a]	2.03 ± 0.6[a]	11.0 ± 2.1[a]	4,293 ± 586.9[a]	1.44 ± 0.3[a]	303.3 ± 20.7	6
EAM+BML	0.99 ± 0.2[b]	1.05 ± 0.4[c]	8.1 ± 1.2[c]	2,600 ± 824.7[b]	0.64 ± 0.2[b]	301.0 ± 21.2	6

Data show mean values ± SD. *Nppa* codes for atrial natriuretic peptide. [a]$P < 0.001$ versus Ctrl+Veh. [b]$P < 0.001$. [c]$P < 0.01$ versus EAM+Veh.

BML = 5(S), (6)R, 7-trihydroxyheptanoic acid methyl ester; Ctrl = control; EAM = experimental autoimmune myocarditis; FI = fold induction; HR = heart rate; HW/TL = heart weight/tibia length; Veh = vehicle.

inflammatory cytokines *Il1b* and *Tnfa* was also significantly higher in EAM+Veh mice than in Ctrl+Veh mice (**Table 1**), corroborating the proinflammatory cardiac environment. By contrast, EAM mice treated with BML-111 (EAM+BML) did not exhibit immune cell infiltration or elevated cardiac inflammatory biomarkers (**Figure 1B, Table 1**), and the mean values of all the parameters were similar to those in control mice treated with BML-111 (Ctrl+BML).

As myocarditis is commonly associated with cardiac dysfunction and hypertrophy, we used transthoracic echocardiography to assess whether BML-111 treatment could improve these outcomes in EAM-induced mice. As expected, mean ejection fraction and fractional shortening were both significantly lower without changes to heart rate in EAM+Veh mice than in Ctrl+Veh mice (**Figure 1C, Table 1,** Supplemental Figure 2), and these functional changes were accompanied by cardiac and cellular hypertrophy, as illustrated by an increase in the heart weight–tibia length ratio, cardiomyocyte surface area, and cardiac *Nppa* messenger RNA (mRNA) levels in EAM+Veh mice (**Table 1**). By contrast, treatment with BML-111 prevented cardiac dysfunction (**Figure 1C,** Supplemental Figure 2) and cardiac and cellular hypertrophy development (**Table 1**) in EAM-induced mice, with similar mean values of all parameters in Ctrl+BML and EAM+BML groups. Additionally, BML-111 administration prevented both the increase in collagen deposition and the higher expression of *Tgfb1*, *Col1a1,* and *Col3a1* induced by EAM (Supplemental Figure 3, Supplemental Table 1). Furthermore, plasma levels of LXA4 were determined in all experimental groups. Supplemental Figure 4 shows increased values in EAM-Veh and EAM-BML groups compared with in the Ctrl-Veh group. Finally, cardiac expression of key enzymes of the biosynthesis of the LXA4 pathway was determined in all groups. Results indicated no significant changes in mRNA levels of *Fpr2/Alx*, *Alox5, Alox12,* and *Alox15* between groups (Supplemental Figure 5). Overall, these data demonstrate that BML-111 prevents cardiac inflammation and functional and structural heart remodeling induced by EAM.

BML-111 COUNTERACTS THE IMPAIRMENT IN SYSTOLIC, DIASTOLIC Ca²⁺ RELEASE AND SR-Ca²⁺ LOAD INDUCED BY EAM. Because cardiac dysfunction is closely related to Ca²⁺ mishandling,[12] we next analyzed EC-coupling in isolated cardiomyocytes. We first questioned whether the Ca²⁺ influx into cardiomyocytes through L-type Ca²⁺ channels was altered by EAM, finding that the mean value of the current-voltage density curves for influx into cardiomyocytes through L-type Ca²⁺ channels was similar among the 4 experimental groups (**Figure 1D**). We next recorded systolic Ca²⁺ release by measuring Ca²⁺ transients elicited in 2 Hz-paced cardiomyocytes. Representative images of the Ca²⁺ transient recordings and the corresponding profile of each experimental group are shown in **Figure 1E**. Results showed that BML-111 administration significantly attenuated the decrease in amplitude (**Figure 1F**, left panel) and the slower time decay of Ca²⁺ transients (**Figure 1F**, center panel) induced by EAM, and improved the cell shortening (**Figure 1F**, right panel). We hypothesized that the slower kinetics of Ca²⁺ transients in the EAM+Veh group may be caused by an impairment of SERCA2A pump function. Indeed, the rate of Ca²⁺ uptake was significantly higher in the EAM+Veh group than in the Ctrl+Veh group, whereas values in the EAM+BML and Ctrl+BML groups were similar and lower than the values in the EAM+Veh group (Supplemental Figure 6). We examined whether the functional alterations in SR-Ca²⁺ uptake were associated with changes in the expression of SERCA2A. Cardiac mRNA levels of SERCA2A (*Atp2a2*) were significantly lower in the EAM+Veh group than in the Ctrl+Veh group, but they were similar between the EAM+BML and Ctrl+Veh groups (**Figure 2A**, left), indicating that BML-111 blunted the down-regulation of *Atp2a2* expression in EAM-induced mice. Proteomic analysis corroborated the gene expression results (**Figure 2A**, right). By contrast, no changes between groups were observed in the phosphorylation state of the key regulator of SERCA2A,

FIGURE 2 BML-111 Treatment Normalizes SR-Ca^{2+} Load, *Atp2a2* Down-Regulation, and Diastolic Ca^{2+} Release in EAM-Induced Mice
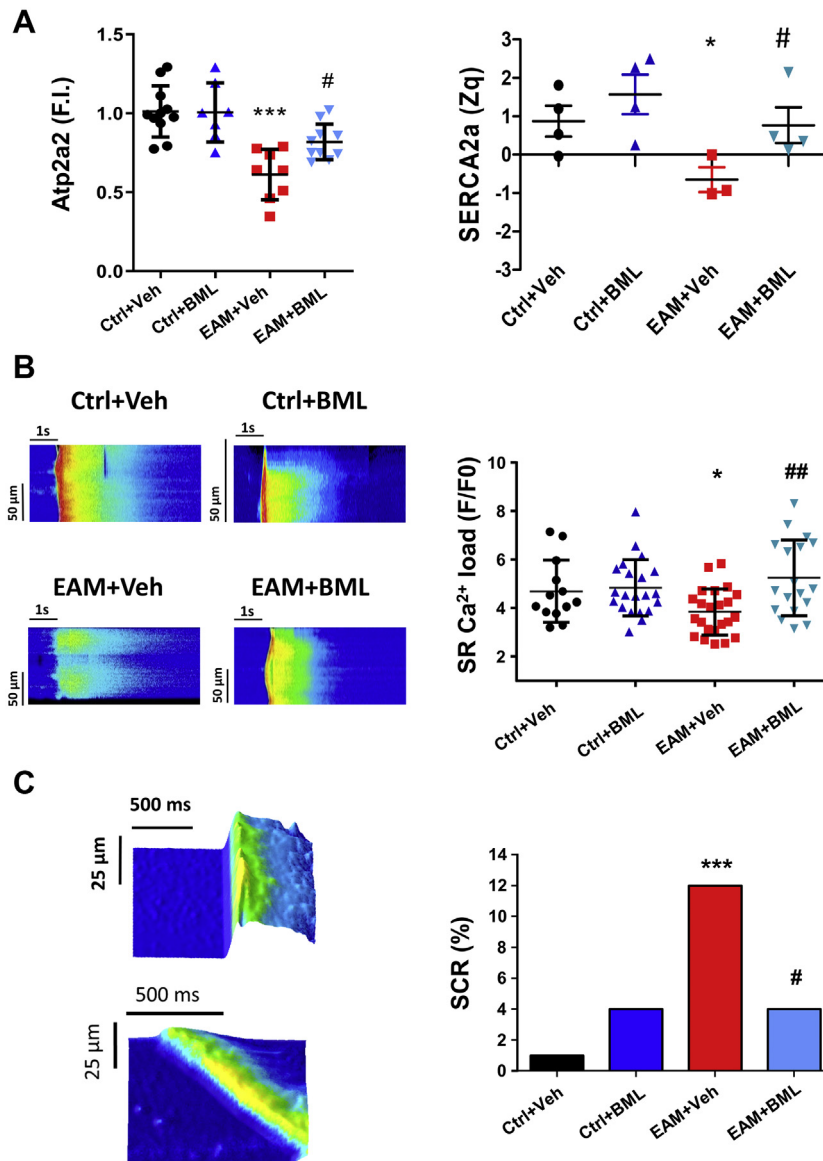

(A, left) Individual and mean values of cardiac levels of *Atp2a2* from Ctrl+Veh (N = 11), Ctrl+ BML (N = 7), EAM+Veh (N = 8), and EAM+BML (N = 10) mice. **(Right)** Relative quantification of sarcoplasmic reticulum–adenosine triphosphatase 2A (SERCA2A) by proteomics; *Zq* values are log$_2$ ratios expressed in SD units (see methods). **(B, left)** Representative line-scan images of caffeine-induced Ca^{2+} transients from all experimental groups. **(Right)** Individual and mean values of the amplitude of caffeine-induced Ca^{2+} transients (F/F0) in cardiomyocytes from Ctrl+Veh (N = 13, N = 5), Ctrl+BML (N = 22, N = 4), EAM+Veh (N = 23, N = 3), and EAM+BML (N = 18, N = 3) mice. **(C, left)** Representative 3-dimensional line-scan confocal images of spontaneous diastolic Ca^{2+} release (SCR) recordings (spontaneous Ca^{2+} transients release **[upper]** and Ca^{2+} waves **[lower]**) from EAM+Veh cardiomyocytes. **(Right)** SCR occurrence in cardiomyocytes from Ctrl+Veh (N = 14, N = 5), Ctrl+BML (N = 19, N = 5), EAM+Veh (N = 21, N = 3), and EAM+BML (N = 24, N = 4) mice. Data show individual values and mean ± SD. *P < 0.05 and ***P < 0.001 versus EAM+Veh; and #P < 0.05 and ##P < 0.01 versus EAM+Veh. Abbreviations as in **Figure 1**.
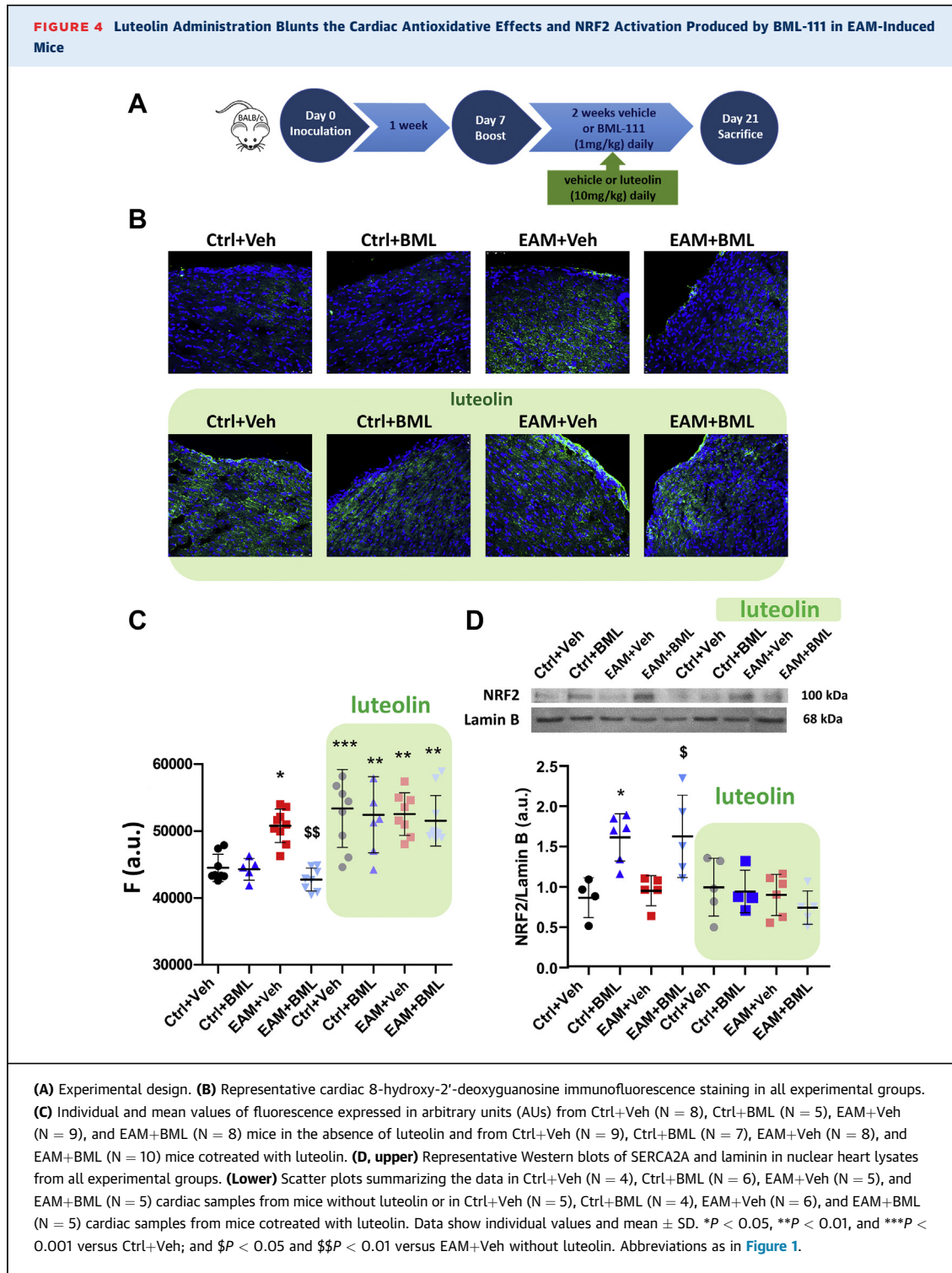
phospholamban, neither in Ser 16 nor in Thr 17 sites (Supplemental Figure 7).

Because the observed impairment in systolic Ca^{2+} release and SERCA2A could also be related to changes in the SR-Ca^{2+} load, we estimated the total SR-Ca^{2+} load as caffeine-evoked Ca^{2+} transients. Representative images of these recordings are shown in the left panel of **Figure 2B**. Results indicated that

FIGURE 3 Comparative Proteomics Analysis Reveals Coordinated Protein Abundance Changes in the Heart Proteome of EAM-Induced Mice After BML-111 Treatment
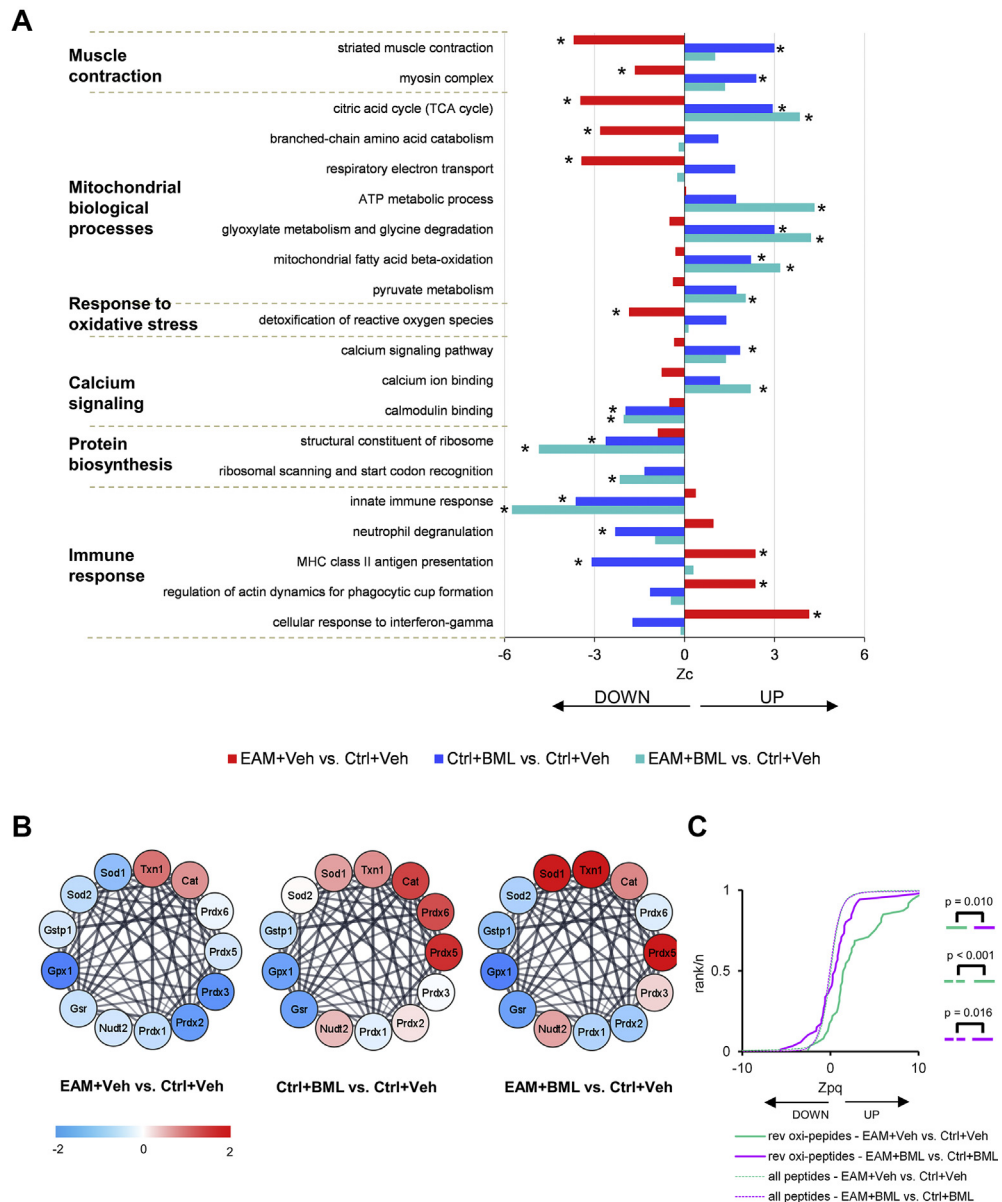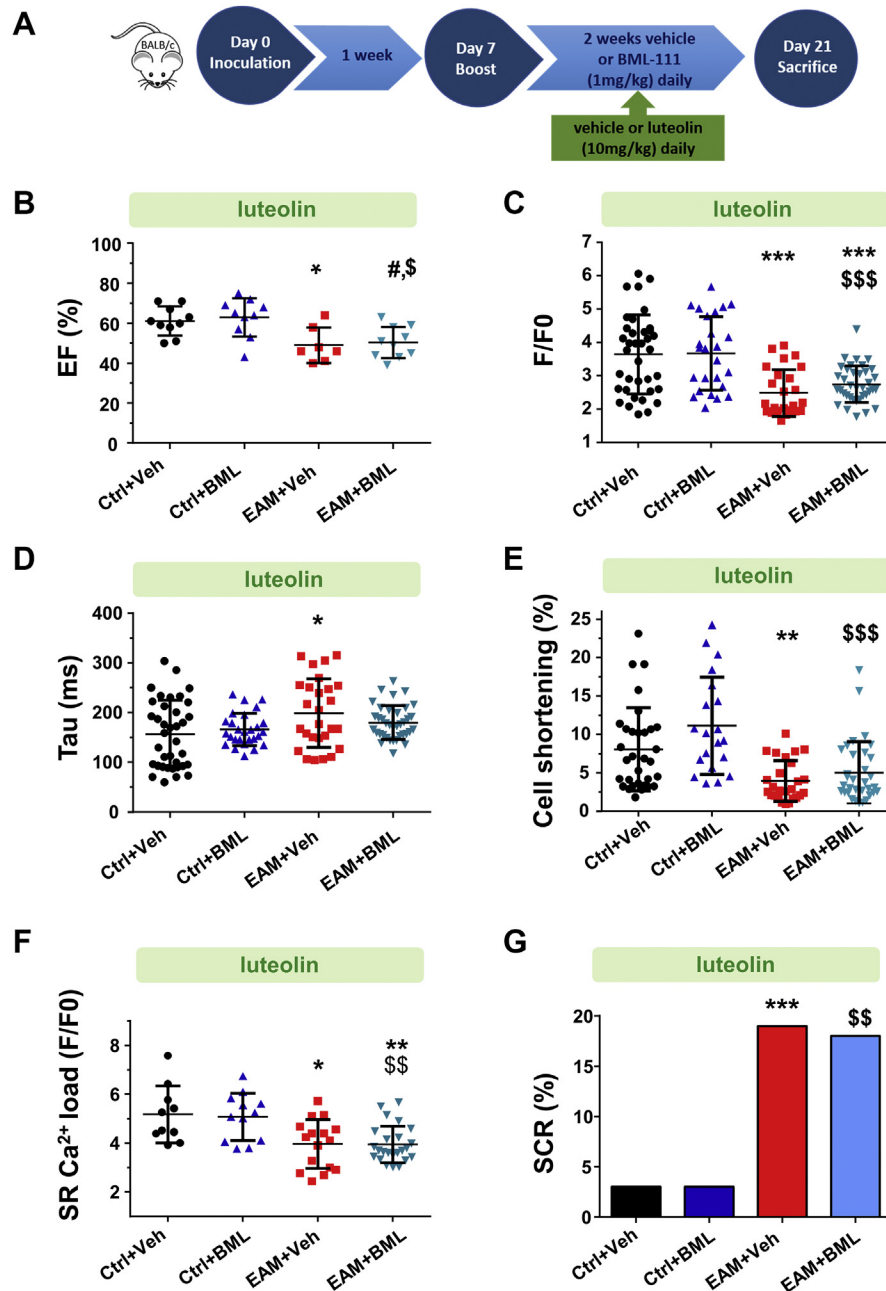

(A) Functional categories significantly altered (*false discovery rate <0.05) in the EAM+Veh, Ctrl+BML, and EAM+BML groups with respect to Ctrl+Veh (control). The Systems Biology Triangle algorithm was used to detect coordinated protein changes by BML-111 treatment. Proteins were functionally annotated using Gene Ontology, Kyoto Encyclopedia of Genes and Genomes, and Reactome terms retrieved from the Uniprot repository. *Zc* values are log₂ ratios of categories expressed in units of SD. Supplemental Table 4 displays *Zq* values for the protein components of the functional categories that were significantly altered. **(B)** Relative quantification of the proteins making up the "response to oxidative stress" category showing a highly interconnected network. Protein-protein associations were taken from the STRING database.[33] **(C)** Redox proteomics analysis using the filter-aided stable isotope labeling of oxidized cysteine (Cys) method detects a significant increase in reversible Cys oxidation levels in the heart proteome in the comparisons EAM+Veh versus Ctrl+Veh and EAM+BML versus Veh+BML groups taking as reference the global behavior of all the peptides from the proteome, which follows the expected null hypothesis. The increase in oxidation level was significantly lower when comparing the modified Cys-containing peptide abundance changes from untreated animals (EAM+Veh vs Ctrl+Veh) with the corresponding BML-treated animals (EAM+BML vs Ctrl+BML). The cumulative distribution of *Zpq* values for the total and the modified Cys-containing peptides is shown. ATP = adenosine triphosphate; MHC = major histocompatibility complex; TCA = tricarboxylic acid; other abbreviations as in **Figure 1**.

FIGURE 4   **Luteolin Administration Blunts the Cardiac Antioxidative Effects and NRF2 Activation Produced by BML-111 in EAM-Induced Mice**

(A) Experimental design. (B) Representative cardiac 8-hydroxy-2′-deoxyguanosine immunofluorescence staining in all experimental groups. (C) Individual and mean values of fluorescence expressed in arbitrary units (AUs) from Ctrl+Veh (N = 8), Ctrl+BML (N = 5), EAM+Veh (N = 9), and EAM+BML (N = 8) mice in the absence of luteolin and from Ctrl+Veh (N = 9), Ctrl+BML (N = 7), EAM+Veh (N = 8), and EAM+BML (N = 10) mice cotreated with luteolin. (D, upper) Representative Western blots of SERCA2A and laminin in nuclear heart lysates from all experimental groups. (Lower) Scatter plots summarizing the data in Ctrl+Veh (N = 4), Ctrl+BML (N = 6), EAM+Veh (N = 5), and EAM+BML (N = 5) cardiac samples from mice without luteolin or in Ctrl+Veh (N = 5), Ctrl+BML (N = 4), EAM+Veh (N = 6), and EAM+BML (N = 5) cardiac samples from mice cotreated with luteolin. Data show individual values and mean ± SD. *P < 0.05, **P < 0.01, and ***P < 0.001 versus Ctrl+Veh; and $P < 0.05 and $$P < 0.01 versus EAM+Veh without luteolin. Abbreviations as in **Figure 1**.

the amplitude of caffeine-evoked Ca²⁺ transients was significantly lower in cardiomyocytes from EAM+Veh mice than from Ctrl+Veh mice (**Figure 2B**, right). By contrast, the amplitude of caffeine-evoked Ca²⁺ transients was similar between cardiomyocytes

from EAM+BML mice and Ctrl-BML mice and comparable to those from Ctrl+Veh mice.

Changes in SR-Ca²⁺ load are often related to aberrant diastolic Ca²⁺ release. To question this possibility, we analyzed the frequency of small Ca²⁺ leakage

FIGURE 5 Luteolin Blocks the Improvement in Cardiac Function and Ca²⁺ Dynamics Produced by BML-111 in EAM-Induced Mice

(A) Experimental design. (B) Plots illustrate individual and mean values of EF in Ctrl+Veh (N = 10), Ctrl+ BML (N = 10), EAM+Veh (N = 7), and EAM+BML (N = 10) mice treated with luteolin. (C-E) Individual and mean values of peak fluorescence Ca²⁺ transients (C), decay time constant (D), and cell shortening (E) in cardiomyocytes from Ctrl+Veh (N = 36, N = 4), Ctrl+BML (N = 25, N = 4), EAM+Veh (N = 26, N = 4), and EAM+BML (N = 37, N = 4) from luteolin-treated mice. Data show individual values and mean ± SD. (F) Individual and mean values of the amplitude of caffeine-induced Ca²⁺ transients (F/FO) in cardiomyocytes from Ctrl+Veh (N = 10, N = 4), Ctrl+BML (N = 12, N = 4), EAM+Veh (N = 16, N = 4), and EAM+BML (N = 24, N = 4) mice treated with luteolin. (G) Graph shows SCR occurrence in cardiomyocytes from Ctrl+Veh (N = 10, N = 4), Ctrl+BML (N = 12, N = 4), EAM+Veh (N = 16, N = 4), and EAM+BML (N = 24, N = 4) mice treated with luteolin. Data show individual values and mean ± SD. *$P < 0.05$, **$P < 0.01$, and ***$P < 0.001$ versus Ctrl+Veh; and $P < 0.05$, $$P < 0.01$, and $$$P < 0.001$ versus Ctrl+BML. SR = sarcoplasmic reticulum; other abbreviations as in **Figures 1 and 2**.

in the form of Ca^{2+} sparks in quiescent cells. We found no changes in the number of these events among the 4 experimental groups (Supplemental Figure 8); however, other proarrhythmogenic forms of spontaneous diastolic Ca^{2+} release (SCR), such as Ca^{2+} waves and spontaneous Ca^{2+} transients, were significantly higher in the EAM+Veh group than in the Ctrl+Veh group (Figure 2C). Notably, the percentage of SCR in EAM+BML mice (4%) was significantly lower than that in EAM+Veh mice (12%; $P <$ 0.001) (Figure 2C, right), supporting the notion that BML-111 prevents the increased diastolic Ca^{2+} leak induced by EAM. The effects of BML-111 on diastolic Ca^{2+} release may contribute to preserve the SR-Ca^{2+} load at physiological levels, prompting regular systolic Ca^{2+} release in EAM+BML cotreated mice by maintaining SERCA2A physiological levels. These beneficial effects can explain the normal cell contractility and thus cardiac function in EAM mice treated with BML-111.

BML-111 ADMINISTRATION INDUCES A PROTECTIVE EFFECT AGAINST OXIDATIVE STRESS THROUGH NRF2 MODULATION.

We performed high-throughput multiplexed quantitative proteomics analysis to determine whether the beneficial effects of BML-111 on EAM were related to changes in the cardiac protein profile. Analysis of tissue protein extracts (4 animals per group) allowed the quantification of 2,332 proteins with a false discovery rate of 1% (Supplemental Table 2). Application of the Systems Biology Triangle algorithm revealed significant abundance changes in functional categories (false discovery rate <0.05) in EAM+Veh, EAM+BML, and Ctrl+BML mice compared with in Ctrl+Veh mice (Supplemental Table 3). To improve the biological interpretation, we manually grouped the categories into 6 functional clusters (Figure 3A). Muscle contraction and some mitochondrial processes such as tricarboxylic acid cycle, respiratory electron transport, and amino acid metabolism were significantly lower in the EAM+Veh group than in the Ctrl+Veh group. Contrastingly, these functional categories, as well as other mitochondrial processes such as adenosine triphosphate, glyoxylate, pyruvate metabolism, and fatty acid β-oxidation were significantly higher in the Ctrl+BML and EAM+BML groups. In addition, proteins involved in the regulation of muscle contraction through the Ca^{2+} signaling pathway were more abundant in the Ctrl+BML and EAM+BML groups. Of note, the immune response cluster was significantly elevated in EAM+Veh mice, but it was diminished in EAM+BML mice and was lower still in Ctrl+BML mice. Taken together, these results suggest that BML-111 can recover myocardial contraction by attenuating the mitochondrial dysfunction induced by EAM and by limiting the exacerbated autoimmune response.

Myocarditis is associated with increased oxidative stress. To further explore the protective function of BML-111 against oxidative stress, we focused on the "response to oxidative stress" functional category, which was significantly lower in EAM+Veh mice than in Ctrl+Veh mice (Figure 3A). Proteins implicated in cellular reactive oxygen species removal such as Sod1, Txn1, Cat, and Prdx5 were increased in abundance in both EAM+BML and Ctrl+BML mice (Figure 3B), suggesting that BML-111 stimulates the activity of these detoxifying enzymes. In addition, we analyzed the heart tissue "redoxome" by quantitating the reversible Cys oxidation levels in the 4 experimental groups using the filter-aided stable isotope labeling of oxidized Cys method. We observed a significantly higher abundance of oxidized Cys-containing peptides in EAM+Veh mice than in Ctrl+Veh mice. The levels of reversible Cys oxidation were significantly lower in BML-111-treated animals (Figure 3C), highlighting the protective role of BML-111 against oxidative damage in the heart.

Next we explore in-depth the elevated oxidative stress environment in the EAM model. We determined cardiac oxidative stress by staining for the oxidative DNA damage biomarker 8-hydroxy-2'-deoxyguanosine (8-OHdG), finding that 8-OHdG cardiac staining was significantly greater in EAM+Veh mice than in Ctrl+Veh mice (Figures 4A-4C). As anticipated, 8-OHdG staining in the myocardium was significantly lower in EAM+BML mice than in EAM+Veh mice (Figures 4B and 4C). As many of the beneficial antioxidant actions of lipoxins are mediated through NRF2 activation, we determined its activation by analyzing its nuclear accumulation in heart. We found that nuclear levels of NRF2 were significantly higher in myocardium of BML-111-treated mice (in both Ctrl and EAM-induced mice) than in nontreated mice (Figure 4D), supporting the notion that BML-111 prevents myocarditis-induced oxidative stress by activating NRF2. We also performed a series of experiments in EAM-induced mice coadministered with luteolin, a compound that can induce oxidative stress through inhibition of the NRF2 pathway (schema in Figure 4A).[13] Luteolin coadministration blunted the protective effects of BML-111 on oxidative stress, as shown by a significant increase in 8-OHdG staining in the myocardium of Ctrl and EAM-induced mice treated with BML-111 (Figures 4B and 4C). Additionally, luteolin

counteracted the increase in cardiac nuclear NRF2 levels induced by BML-111 administration in both Ctrl and EAM groups (**Figure 4D**). Overall, these data indicate that luteolin blocks BML-111-induced activation of NRF2 in the myocardium, thus preventing the protective action of BML-111 against cardiac oxidative stress. These results point to luteolin as a useful tool to determine the role of NRF2 in Ca^{2+} mishandling showed in our EAM model.

LUTEOLIN ADMINISTRATION BLUNTS THE PROTECTIVE EFFECTS OF BML-111 ON CARDIAC FUNCTION AND INTRACELLULAR Ca^{2+} DYNAMICS IN EAM-INDUCED MICE.

We next questioned whether luteolin lessens the protective effects of BML-111 on cardiac function and intracellular Ca^{2+} handling in EAM-induced mice (schema in **Figure 5A**). The values for ejection fraction and fractional shortening in EAM-induced mice cotreated with BML-111 and luteolin (EAM+Lut+BML) were similar to those found in EAM+Lut mice and were significantly lower than those of Ctrl mice (**Figure 5B,** Supplemental Figure 9).

At the cellular level, luteolin coadministration dampened the protective effect of BML-111 on systolic Ca^{2+} release and SR-Ca^{2+} load in cardiomyocytes. Indeed, the depressed amplitude of Ca^{2+} transients and cell shortening, as well as the low SR-Ca^{2+} load, in the EAM+Lut group was maintained in the EAM+Lut+BML group (**Figures 5C to 5F**). Of note, the administration of luteolin sustained the slower Ca^{2+} transient kinetics (**Figure 5D**), indicating that SER-CA2A impairment was maintained in EAM+Lut+BML mice. Supporting these findings, we found higher values for Ca^{2+} uptake rate in cells from EAM-Lut group compared with the Ctrl group, and the coadministration of BML-111 was unable to reverse this increase (Supplemental Figure 10). Finally, the increased SCR in EAM+Lut mice (19%) was also evident in EAM+Lut+BML mice (18%) (**Figure 5G**). Overall, these results suggest that NRF2 might be a key player in the protective effects of BML-111 on cardiac dysfunction and intracellular Ca^{2+} mishandling induced by EAM.

GENETIC DELETION OF NRF2 AVERTS THE IMPROVEMENT IN Ca^{2+} HANDLING INDUCED BY LIPOXINS.

To definitively determine whether NRF2 mediates the effects of SPMs on Ca^{2+} dynamics and to evaluate the direct effect of lipoxins in isolated cardiomyocytes, we conducted a series of experiments using cardiomyocytes isolated from wild-type (*Wt*) and *Nrf2* knockout (*Nrf2*$^{-/-}$) mice. Cells were incubated for 1 hour with Veh or with 250 nmol/L 15-epi-lipoxin A4 (Epi), an LXA4 derivative widely used in in vitro experiments, and systolic Ca^{2+} release and SR-Ca^{2+}

load/uptake were determined. Representative Ca^{2+} transients obtained in each condition are shown in **Figure 6A**. Results showed that acute administration of Epi improved systolic Ca^{2+} release in *Wt* cardiomyocytes, mainly by increasing the amplitude of Ca^{2+} transients (**Figure 6B**, left panel) and accelerating their kinetics (**Figure 6B**, central panel). Also, SR-Ca^{2+} uptake by SERCA2A was improved by Epi treatment (**Figure 6B**, right panel), which can also contribute to increase SR-Ca^{2+} load in *Wt* cells (**Figure 6C**). By contrast, Epi administration to cardiomyocytes from *Nrf2*$^{-/-}$ mice had no effect on systolic Ca^{2+} release or on SR-Ca^{2+} uptake and load (**Figures 6A to 6C**). These results support the notion that NRF2 is a key mediator that improves systolic Ca^{2+} release and SR-Ca^{2+} uptake and load in isolated cardiomyocytes and point to SERCA2A as a target of NRF2 action. Interestingly, the effects induced by Epi on Ca^{2+} handling were blunted in cardiomyocytes cotreated with the selective inhibitor of NRF2, ML-385 (Supplemental Figure 11). Consistent with this idea, we found that cardiac tissue from *Wt* mice previously treated with BML-111 showed elevated protein levels of SERCA2A (**Figure 6D**). To determine whether the observed effects of Epi on Ca^{2+} handling were mediated by FPR2/ALX receptor, cardiomyocytes were cotreated with Epi and the FPR2/ALX antagonist, WRW4, and both systolic Ca^{2+} release and SR-Ca^{2+} load were analyzed. Supplemental Figure 12 shows that WRW4 administration avoided the effects induced by Epi on Ca^{2+} transient amplitude and kinetics and also prevented the modulation of Epi on SR-Ca^{2+} load, suggesting that Epi induces its acute effects on intracellular Ca^{2+} release through FPR2/ALXR. Overall, these results highlight SERCA2A and NRF2 as key modulators of the beneficial effects of SPMs on Ca^{2+} handling.

TRANSCRIPTIONAL ACTIVITY OF NRF2 DETERMINES SERCA2A EXPRESSION IN HUMAN VENTRICULAR CARDIOMYOCYTES.

Having shown that BML-111 modulates murine cardiac SERCA2A expression and that NRF2 appears to be the main contributor of its effects on Ca^{2+} dynamics, we next investigated whether the molecular regulation of *NFE2L2* (NRF2 coding gene) determines SERCA2A expression. We evaluated SERCA2A expression in a human ventricular cardiomyocyte cell line (AC16) silenced for *NFE2L2* expression or overexpressing *NFE2L2*. Results showed that the down-regulation of *NFE2L2* in AC16 cells impaired the expression of its canonical targets (HMOX1 and NQO1) and also decreased the expression of SERCA2A (**Figure 7A**). Conversely, the

FIGURE 6 Genetic Deletion of *Nrf2* Tempers the Elevated Systolic Ca^{2+} Release and SR-Ca^{2+} Load and Uptake Induced by Epi in Isolated Cardiomyocytes
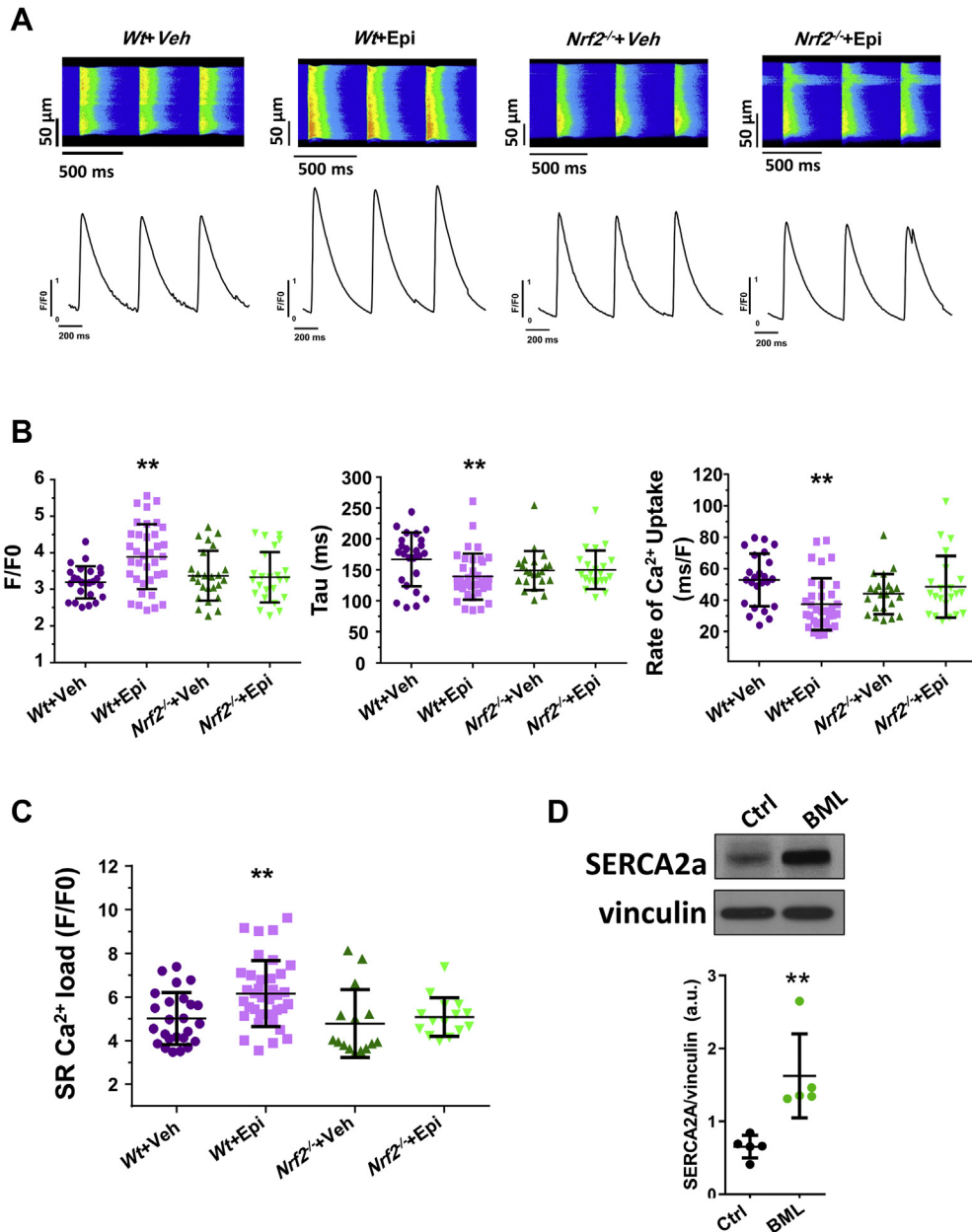
Cardiomyocytes from wild-type (WT) and *Nrf2* knockout (*Nrf2$^{-/-}$*) mice were incubated for 1 hour with Veh or 250 nmol/L 15-epi-lipoxin A4 (Epi). **(A)** Representative line-scan confocal images and the corresponding profiles of Ca^{2+} transients from 1 cell in each experimental group. **(B)** Individual and mean values of peak fluorescence Ca^{2+} transients **(left)**, decay time constant (Tau) **(center)**, and the rate of Ca^{2+} uptake **(right)** in WT+Veh (N = 25, N = 4); WT+Epi (N = 36, N = 4), *Nrf2$^{-/-}$*+Veh (N = 22, N = 3) and *Nrf2$^{-/-}$*+Epi (N = 24, N = 3) cardiomyocytes. **(C)** Individual and mean values of the amplitude of the caffeine-induced Ca^{2+} transients (F/F0) obtained in WT+Veh (N = 26, N = 4), WT+Epi (N = 36, N = 4), *Nrf2$^{-/-}$*+Veh (N = 15, N = 3), and *Nrf2$^{-/-}$*+Epi (N = 15, N = 3) cells. Data show individual values and mean ± SD. **P < 0.01 versus WT+Veh. **(D, upper)** Representative Western blots of SERCA2A and vinculin from cytosolic heart lysates from WT mice treated with Veh (Ctrl) or BML-111 (BML) for 6 hours. **(Lower)** Scatter plots summarizing the data in Ctrl (N = 4) and BML-111–treated (N = 5) mice expressed as arbitrary units. Data show individual values and mean ± SD. *P < 0.01 versus Ctrl. Abbreviations as in Figures 1, 2, and 5.

FIGURE 7   Correlation Between NRF2 and SERCA2A2 Expression in Human Ventricular Cells and in Myocardium From Patients With Myocarditis
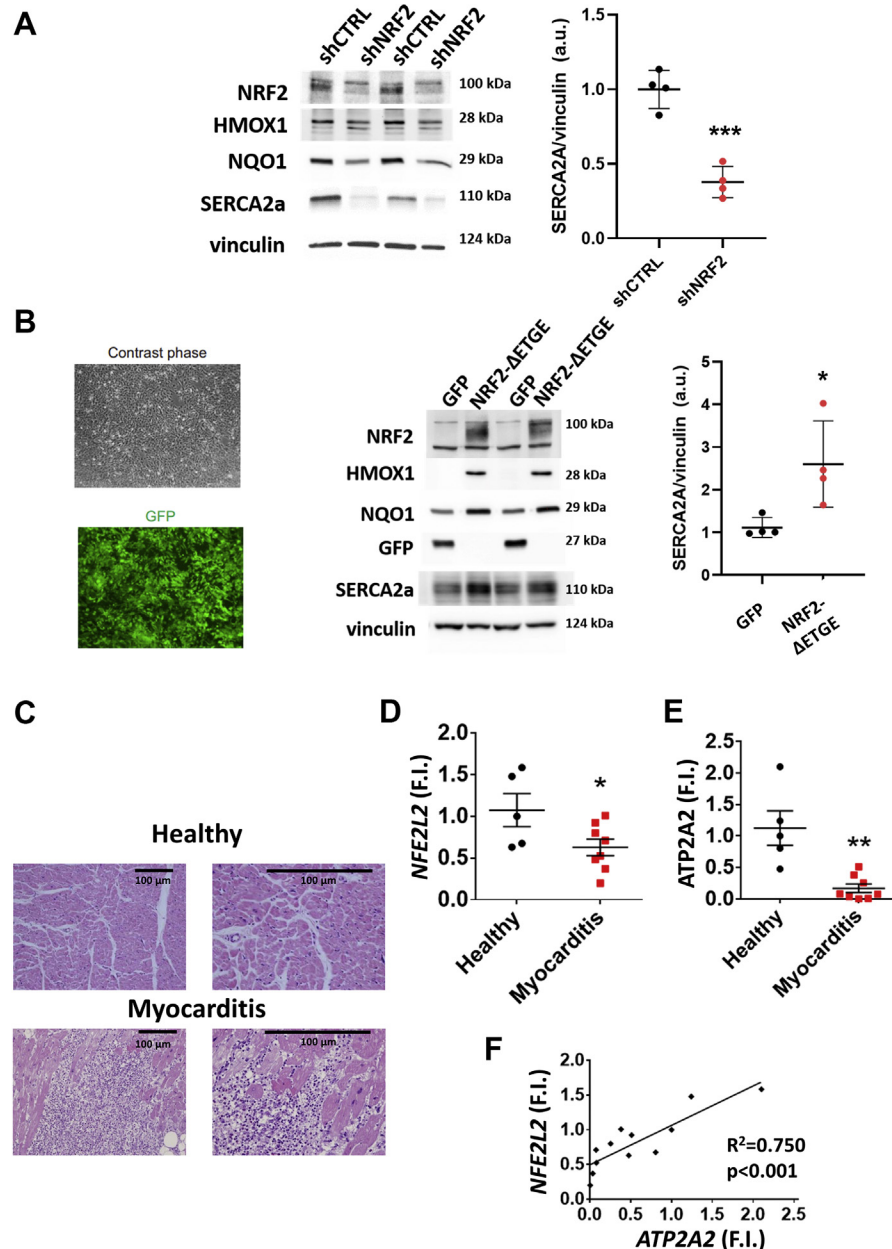
(A) AC16 cells were transduced with a lentivirus carrying a short hairpin RNA (shRNA) against a scramble sequence (shCTRL) or against NRF2 (shNRF2). (Left) Representative Western blots of the indicated proteins were determined 7 days post-transduction. Vinculin was used as loading control. (Right) Densitometry quantification of SERCA2A protein levels normalized to vinculin levels. Data are mean ± SD (N = 4). ***P < 0.001 versus shCTRL transduced cells. (B) AC16 cells were transduced with a lentivirus expressing green fluorescent protein (GFP) or a constitutive active version of NRF2 (NRF2-ΔETGE). (Left) Representative images showing efficient transduction 4 days post-lentivirus delivery. (Center) Representative Western blots of the indicated proteins (NRF2, HMOX1, NQO1, GFP, and SERCA2A) were determined 4 days post-transduction. Vinculin was used as a loading control. (Right) Densitometry quantification of SERCA2A protein levels normalized to vinculin levels. Data are mean ± SD (N = 4). *P < 0.05 and ***P < 0.001 versus GFP transduced cells. (C, left) Representative hematoxylin and eosin–stained slides of healthy myocardium (N = 5) and myocardium from patients with myocarditis (N = 8). Original magnification ×10 (right) and ×20 (left). (D, E) Individual and mean values of messenger RNA levels of *NFE2L2* (D) and *ATP2A2* (E) normalized to human 36B4. (F) Pearson correlation analysis of *ATP2A2* and *NFE2L2* messenger RNA levels in human samples. A linear regression of the data is shown. Data show individual values and mean ± SD.*P < 0.01 and **P < 0.01 versus healthy group. FI = fold induction; other abbreviations as in **Figures 1 and 2**.

overexpression of NRF2 increased SERCA2A protein levels (**Figure 7B**). These results strongly suggest that the modulation of *NFE2L2* determines SERCA2A expression in human ventricular cardiomyocytes.

HUMAN MYOCARDIUM FROM PATIENTS WITH MYOCARDITIS HAS LOW NFE2L2 AND ATP2A2 EXPRESSION.

To translate the main results to the human heart, we examined human myocardium from patients with myocarditis. Samples of healthy and myocarditis-positive myocardium were characterized by immunostaining. Representative examples of hematoxylin-eosin staining of healthy cardiac tissue and tissue from patients with a clinical diagnosis of myocarditis are shown in **Figure 7C**, with evident immune cell infiltration and tissue damage in the latter (Supplemental Figure 13). Analysis of *NFE2L2* expression revealed significantly lower myocardial levels in patients with myocarditis than in healthy samples (**Figure 7D**).

As Ca²⁺ mishandling in the EAM model was closely related to impairment in SERCA2A, we also analyzed *ATP2A2* mRNA levels in human myocardium tissue. Results showed that *ATP2A2* expression was significantly lower in myocarditis-positive myocardium than in healthy cardiac tissue (**Figure 7E**).

Finally, correlation analysis revealed a strong and direct association between *NFE2L2* and *ATP2A2* expression (**Figure 7F**). These results support our findings in the EAM model, showing a significant impairment of NRF2 and SERCA2A expression and reveal an interconnection between them. By contrast, no changes were found in the expression of *FPR2/ALX* or in the key enzymes of the biosynthesis of the LXA4 pathway between groups (Supplemental Figure 14). Overall, our findings identify NRF2 and SERCA2A as novel partners in the functional cardiac remodeling linked to myocarditis.

DISCUSSION

Myocarditis is a complex inflammatory disease affecting the myocardium that is triggered by both infectious and noninfectious agents and leads, in many cases, to dilated cardiomyopathy, with a 1-year mortality rate of 15%-20%.[14] The lack of specific treatments for myocarditis adds to the challenges of managing patients with this disease and highlights the need to identify new targets and mechanisms to develop future treatments.

SPMs are potential therapeutic tools for treating cardiovascular diseases with a clear inflammatory component, such as myocarditis, as they can drive the resolution of inflammation to recover a healthy state. Administration of SPMs in various experimental models exerts protective cardiac effects, including halting inflammatory responses, cell death, oxidative stress, and fibrosis development, ultimately improving cardiac function in myocarditis and other cardiovascular diseases.[8,15]

The potential utility of lipoxins is limited by their short half-life, which has prompted the development of new synthetic drugs such as BML-111, an LXA4 receptor agonist with improved stability and potency. BML-111 has proved effective against different inflammatory diseases, but relatively little is known about its specific cardiac effects. Our study demonstrates that BML-111 administration prevents both structural and functional cardiac remodeling associated with myocarditis in a model of EAM, with functional amelioration closely related to the protection against cardiomyocyte Ca²⁺ mishandling. Specifically, BML-111 treatment prevented the reduced systolic Ca²⁺ release and diminished SR-Ca²⁺ uptake induced by EAM. One of the main protective mechanisms elicited by BML-111 involved the preservation of SERCA2A protein levels, preventing its downregulation on EAM induction. The maintenance of physiological levels of SERCA2A was pivotal to sustain an adequate SR-Ca²⁺ load, thus contributing to preserve cell contractility and cardiac function in EAM mice treated with BML-111.

Disruptions in EC-coupling can also involve diastolic Ca²⁺ leak through ryanodine receptors in many cardiovascular diseases.[16] Diastolic Ca²⁺ leak in the form of SCR was evident in cardiomyocytes from EAM-induced mice, and these aberrant proarrhythmogenic events were averted by administered BML-111. The beneficial effects of BML-111 on diastolic Ca²⁺ release together with the maintenance of SERCA2A activity contribute to preserve the SR-Ca²⁺ load at physiological levels, prompting regular systolic Ca²⁺ release and cell contractility in EAM+BML-treated mice. All of these functional results were corroborated by the proteomics analysis, which indicated that the beneficial effects of BML-111 on cardiac function and structure were associated with the prevention of EAM-induced changes in proteins involved in contraction, energy regulation, and Ca²⁺ dynamics. Interestingly, the administration of BML-111 did not modify cardiac expression of *FPR2/ALXx* receptor or key enzymes of the lipoxin pathway. In contrast, in vitro experiments demonstrated that the treatment of cardiomyocytes with an antagonist of FPR2/ALXR significantly blunted the beneficial effects induced by Epi in systolic Ca²⁺ release and SR-Ca²⁺ load, suggesting that the functional effect of SPMs requires FPR2/ALXR to modulate intracellular Ca²⁺ handling. In this line, an interesting study carried out by Petri

et al[17] pointed to FPR2/ALXR as a main player in the murine atherosclerosis progression.

Our results indicate that SERCA2A is fundamental for BML-111–induced prevention of Ca²⁺ mishandling, pointing to this SR-adenosine triphosphatase as an excellent candidate to develop new therapies that improve cardiac function in patients with myocarditis. Indeed, *SERCA2A* gene therapy has been evaluated in clinical trials for heart failure[18,19] and in preclinical experimental small and large animal models, which show improvements in myocardial contractility.[20,21] However, discrepancies regarding the beneficial role of targeting SERCA2A were found in the CUPID (Calcium Upregulation by Percutaneous Administration of Gene Therapy in Cardiac Disease) trials,[19,22] which might be explained by the possible low efficiency of gene transduction or possibly by post-translational regulatory factors of SERCA2A in human heart failure. In this regard, our results uncover NRF2 as a key modulator of the expression of SERCA2A in human cardiac cells, supporting an emergent field for clinical research in myocarditis or other cardiovascular diseases such as heart failure that are associated with a clear down-regulation of the SR-adenosine triphosphatase.

NRF2 is a master antioxidant factor that has recently gained much interest in cardiac disease research[23-25] because of its antioxidant and anti-inflammatory effects. Our results show that the protective effect of BML-111 on cardiac function and Ca²⁺ handling is related to the promotion of NRF2 activation. Functional Ca²⁺ analysis revealed that pharmacologic blockade of NRF2 in EAM-induced mice blunted the improvement in the intracellular Ca²⁺ handling induced by the SPM, with evident harmful effects on cardiac function, and these findings were mirrored in in vitro studies on cardiomyocytes from *Nrf2*⁻/⁻ mice and cells treated with a selective inhibitor of NRF2. Supporting our data, other studies have reported that genetic deletion or pharmacologic blockade of NRF2 contributes to harmful structural and functional cardiac remodeling by augmenting oxidative stress and the inflammatory response.[26-28]

Regarding the specific role of NRF2 in the regulation of Ca²⁺ handling, we found that NRF2 activation by BML-111 in mice or its overexpression in human ventricular cells increased SERCA2A expression, suggesting that the SR-Ca²⁺ pump is a direct or indirect downstream target of NRF2. Indeed, in preliminary results we have searched the ENCODE database for NRF2-binding enhancer, antioxidant response element (called ARE). Although this database does not report information about NRF2 chromatin immunoprecipitations, other ARE-binding proteins such as MAFF, MAFK, and BACH1 were found to bind the *ATP2A2* gene at 16 sites located at H3K27Ac and DNAse sensitive sites, consistent with promoter regulatory regions (Supplemental Figure 15).

Supporting our hypothesis was the finding that down-regulation of *NFE2L2* in human cells was associated with a decrease in SERCA2A. BML-111–activated NRF2 triggers the maintenance of SERCA2A levels in a physiological range, improving SR-Ca²⁺ uptake and promoting systolic Ca²⁺ release and cardiomyocyte contraction. All of these beneficial effects of BML-111 contributed to prevent the cardiac dysfunction in EAM-induced mice. In line with our results, Erkens et al[26] demonstrated that *Nrf2*⁻/⁻ mice present cardiac dysfunction associated with a down-regulation of SERCA2A. Concerning the inflammatory environment and cardiac NRF2 and SERCA2A regulation, Bai et al[29] described that the administration of a strong proinflammatory stimulus (lipopolysaccharide) to mice promoted both cardiac SERCA2A and NRF2 down-regulation, and both processes were attenuated in the presence of the antioxidant resveratrol.

Validating the main findings of our experimental model, we found a down-regulation of both *NFEL2F* and *ATP2A2* expression in human myocarditis-positive myocardium, and a significant correlation between the expression of both molecules, pointing to an interconnection between them in human myocarditis. In relation to possible translation of findings to human pathology, it is important to mention that myocarditis has also recently been described as a potential complication of COVID-19,[30] and cardiac damage and dysfunction induced by myocarditis have been observed in patients both in hospital and over the long term.[31] Interestingly, a recent lipidomic analysis showed that patients with severe COVID-19 had significantly lower levels of SPMs (resolvins E3) than did peers with moderate disease,[32] indicating that the loss of SPMs might be associated with the more severe form of COVID-19. Our data may provide a new research direction focused on NRF2-SERCA2A interventions for the development of specific treatments for myocarditis in general and for cardiac complications in patients with COVID-19.

CONCLUSIONS

Our findings point to SPMs as a new therapeutic alternative for treating myocarditis. Our study uncovers that SPMs induce cardioprotection by regulating cardiac function and intracellular Ca²⁺

dynamics though the modulation of NRF2 and SER-CA2A activation. Our results are particularly relevant for patients with myocarditis in general and also for individuals with COVID-19 and myocarditis, because the employment of specific compounds to promote the resolution phase of the inflammatory response may help to manage the cytokine storm and the consequent tissue damage. Additionally, SPMs can contribute to improve cardiac dysfunction by the amelioration of intracellular Ca²⁺ mishandling, expanding the therapeutic spectrum of these compounds.

ADDRESS FOR CORRESPONDENCE: Dr María Fernández-Velasco, Instituto de Investigación Hospital la Paz, IdiPAZ, Paseo de la Castellana 261, 28046 Madrid. Spain. E-mail: maria.fernandez@idipaz.es OR mvelasco@iib.uam.es. OR Dr Patricia Prieto, Facultad de Farmacia, Universidad Complutense de Madrid, Plaza de Ramón y Cajal s/n, 28040 Madrid, Spain. E-mail: patprio2@ucm.es. OR Dr Lisardo Bosca, Instituto de Investigaciones Biomédicas Alberto Sols (CSIC-UAM), Arturo Duperier 4, 28029 Madrid, Spain. E-mail: lbosca@iib.uam.es.

PERSPECTIVES

COMPETENCY IN MEDICAL KNOWLEDGE: This study uncovers SPMs as new therapeutic tools that target the NRF2-SERCA2A axis with a potential clinical application in the treatment of myocarditis. These results are of special clinical relevance, because *SERCA2A* gene therapy has failed in clinical trials and SPMs support a new system to improve cardiac function by preventing the increased oxidative stress associated not only with myocarditis disease, but also with other cardiac pathologies linked to an increased inflammatory response, such as heart failure.

TRANSLATIONAL OUTLOOK: SPMs emerge as new therapeutic tools with a potential clinical application in the treatment of myocarditis and supporting a new strategy to improve cardiac function in proinflammatory cardiac pathologies.

REFERENCES

1. Kindermann I, Barth C, Mahfoud F, et al. Update on myocarditis. *J Am Coll Cardiol*. 2012;59(9):779–792.

2. Hendren NS, Drazner MH, Bozkurt B, Cooper LT. Description and proposed management of the acute COVID-19 cardiovascular syndrome. *Circulation*. 2020;141(23):1903–1914.

3. Biesbroek PS, Beek AM, Germans T, Niessen HWM, Van Rossum AC. Diagnosis of myocarditis: current state and future perspectives. *Int J Cardiol*. 2015;191:211–219.

4. Ruiz-Hurtado G, Li L, Fernández-Velasco M, et al. Reconciling depressed Ca2+ sparks occurrence with enhanced RyR2 activity in failing mice cardiomyocytes. *J Gen Physiol*. 2015;146(4):295–306.

5. Bers DM. Cardiac excitation-contraction coupling. *Nature*. 2002;415(6868):198–205.

6. Wahlquist C, Jeong D, Rojas-Muñoz A, et al. Inhibition of miR-25 improves cardiac contractility in the failing heart. *Nature*. 2014;508(7497):531–535.

7. Serhan CN, Savill J. Resolution of inflammation: the beginning programs the end. *Nat Immunol*. 2005;6(12):1191–1197.

8. Jaén RI, Fernández-Velasco M, Terrón V, et al. BML-111 treatment prevents cardiac apoptosis and oxidative stress in a mouse model of autoimmune myocarditis. *FASEB J*. 2020;34(8):10531–10546.

9. Lee TH, Lympany P, Crea AE, Spur BW. Inhibition of leukotriene B4-induced neutrophil migration by lipoxin A4: structure-function

relationships. *Biochem Biophys Res Commun*. 1991;180(3):1416–1421.

10. Cuadrado A, Rojo AI, Wells G, et al. Therapeutic targeting of the NRF2 and KEAP1 partnership in chronic diseases. *Nat Rev Drug Discov*. 2019;18(4):295–317.

11. da Costa RM, Rodrigues D, Pereira CA, et al. Nrf2 as a potential mediator of cardiovascular risk in metabolic diseases. *Front Pharmacol*. 2019;10:382.

12. Val-Blasco A, Piedras MJGM, Ruiz-Hurtado G, et al. Role of NOD1 in heart failure progression via regulation of Ca2+ handling. *J Am Coll Cardiol*. 2017;69(4):423–433.

13. Suraweera TL, Vasantha Rupasinghe HP, Dellaire G, Xu Z. Regulation of Nrf2/ARE pathway by dietary flavonoids: A friend or foe for cancer

management? *Antioxidants (Basel)*. 2020;9(10): 973.

14. McCarthy RE, Boehmer JP, Hruban RH, et al. Long-term outcome of fulminant myocarditis as compared with acute (nonfulminant) myocarditis. *N Engl J Med*. 2000;342(10):690–695.

15. Kain V, Ingle KA, Colas RA, et al. Resolvin D1 activates the inflammation resolving response at splenic and ventricular site following myocardial infarction leading to improved ventricular function. *J Mol Cell Cardiol*. 2015;84:24–35.

16. Fernández-Velasco M, Rueda A, Rizzi N, et al. Increased Ca2+ sensitivity of the ryanodine receptor mutant RyR2R4496C underlies catecholaminergic polymorphic ventricular tachycardia. *Circ Res*. 2009;104(2):201–209, 12 pages following 209.

17. Petri MH, Laguna-Fernández A, Gonzalez-Diez M, Paulsson-Berne G, Hansson GK, Bäck M. The role of the FPR2/ALX receptor in atherosclerosis development and plaque stability. *Cardiovasc Res*. 2015;105(1):65–74.

18. Zsebo K, Yaroshinsky A, Rudy JJ, et al. Long-term effects of AAV1/SERCA2a gene transfer in patients with severe heart failure: analysis of recurrent cardiovascular events and mortality. *Circ Res*. 2014;114(1):101–108.

19. Greenberg B, Butler J, Felker GM, et al. Calcium upregulation by percutaneous administration of gene therapy in patients with cardiac disease (CUPID 2): a randomised, multinational, double-blind, placebo-controlled, phase 2b trial. *Lancet*. 2016;387(10024):1178–1186.

20. Miyamoto MI, Del Monte F, Schmidt U, et al. Adenoviral gene transfer of SERCA2A improves left-ventricular function in aortic-banded rats in transition to heart failure. *Proc Natl Acad Sci U S A*. 2000;97(2):793–798.

21. Byrne MJ, Power JM, Preovolos A, Mariani JA, Hajjar RJ, Kaye DM. Recirculating cardiac delivery of AAV2/1SERCA2a improves myocardial function in an experimental model of heart failure in large animals. *Gene Ther*. 2008;15(23): 1550–1557.

22. Hayward C, Banner NR, Morley-Smith A, Lyon AR, Harding SE. The current and future landscape of *SERCA* gene therapy for heart failure: a clinical perspective. *Hum Gene Ther*. 2015;26(5): 293–304.

23. Vashi R, Patel BM. NRF2 in cardiovascular diseases: a ray of hope. *J Cardiovasc Transl Res*. 2021;14(3):573–586.

24. Kang GJ, Kim EJ, Lee CH. Therapeutic effects of specialized pro-resolving lipids mediators on cardiac fibrosis via NRF2 activation. *Antioxidants (Basel)*. 2020;9(12):1259.

25. Milanesi E, Manda G, Dobre M, et al. Distinctive under-expression profile of inflammatory and redox genes in the blood of elderly patients with cardiovascular disease. *J Inflamm Res*. 2021;14: 429–442.

26. Erkens R, Kramer CM, Lückstädt W, et al. Left ventricular diastolic dysfunction in Nrf2 knock out mice is associated with cardiac hypertrophy, decreased expression of SERCA2a, and preserved endothelial function. *Free Radic Biol Med*. 2015;89:906–917.

27. Li J, Ichikawa T, Villacorta L, et al. Nrf2 protects against maladaptive cardiac responses to hemodynamic stress. *Arterioscler Thromb Vasc Biol*. 2009;29(11):1843–1850.

28. Ge C, Hu L, Lou D, et al. Nrf2 deficiency aggravates PM2.5-induced cardiomyopathy by enhancing oxidative stress, fibrosis and inflammation via RIPK3-regulated mitochondrial disorder. *Aging*. 2020;12(6):4836–4865.

29. Bai T, Hu X, Zheng Y, Wang S, Kong J, Cai L. Resveratrol protects against lipopolysaccharide-induced cardiac dysfunction by enhancing SERCA2a activity through promoting the phospholamban oligomerization. *Am J Physiol Heart Circ Physiol*. 2016;311(4):H1051–H1062.

30. Kawakami R, Sakamoto A, Kawai K, et al. Pathological evidence for SARS-CoV-2 as a cause of myocarditis: JACC Review Topic of the Week. *J Am Coll Cardiol*. 2021;77(3):314–325.

31. Fried JA, Ramasubbu K, Bhatt R, et al. The variety of cardiovascular presentations of COVID-19. *Circulation*. 2020;141(23):1930–1936.

32. Schwarz B, Sharma L, Roberts L, et al. Severe SARS-CoV-2 infection in humans is defined by a shift in the serum lipidome resulting in dysregulation of eicosanoid immune mediators. *J Immunol*. 2021;206(2):329–334.

33. Szklarczyk D, Gable AL, Lyon D, et al. STRING v11: Protein-protein association networks with increased coverage, supporting functional discovery in genome-wide experimental datasets. *Nucleic Acids Res*. 2019;47(D1):D607–D613.